

# Self-consistently determining structures of charged defects and defect ionization energies in low-dimensional semiconductors

Guo-Jun Zhu,<sup>1</sup> Ji-Hui Yang <sup>1,\*</sup> and Xin-Gao Gong<sup>1,2</sup>

<sup>1</sup>*Department of Physics, Key Laboratory for Computational Science (MOE), State Key Laboratory of Surface Physics, Fudan University, Shanghai 200433, China*

<sup>2</sup>*Collaborative Innovation Center of Advanced Microstructures, Nanjing 210093, Jiangsu, China*

 (Received 9 January 2020; revised 15 May 2020; accepted 4 June 2020; published 7 July 2020)

Determination of defect ionization energy in low-dimensional semiconductors has been a long-standing unsolved problem in first-principles defect calculations, because the commonly used methods based on the jellium model introduce an unphysical charge density uniformly distributed in the material and vacuum regions, causing the well-known divergence issue of charged defect formation energies. In addition, because of the unphysical jellium charge, how to determine structures of charged defects is also not clear. These two issues pose great challenges in studying defect properties of low-dimensional semiconductors. Here in this work, we combine the jellium framework together with the idea of constraining charge transfer to deal with charged defects in low-dimensional semiconductors by replacing the unphysical jellium background charge density with the band-edge charge density. By doing this, we show that not only the total energy calculation but also the structure relaxation can be self-consistently obtained in one single calculation, thus providing a simple and efficient way to determine the defect ionization energies in low-dimensional semiconductors.

DOI: [10.1103/PhysRevB.102.035202](https://doi.org/10.1103/PhysRevB.102.035202)

## I. INTRODUCTION

Understanding defect behaviors has been at the heart of semiconductor applications, as defects play many important roles in utilizing semiconductor technologies [1–6]. Among all the defect-related properties, defect formation energy and ionization energy (IE) (also known as transition energy level referenced to band edges) are the most important two key quantities: The former determines defect concentration under equilibrium conditions; the latter, defined as the energy cost to get ionized, determines the ability of a defect to provide carriers [2,7–9]. To determine defect IE, both formation energies of neutral and charged defects should be known, which can be obtained from first-principles defect calculations based on density-functional theory (DFT). During the past decades, defect calculations have been widely performed for three-dimensional (3D) systems [8,10–14], which has provided guidance for defect control and engineering to boost the performance and efficiency of many devices [8,15,16].

Usually, a supercell structure model along with periodic boundary conditions (PBCs) is adopted during defect simulations and thus periodic images of defects are also created [17–19]. The key quantity to be obtained through first-principles calculations is the total energy of the supercell with a defect at its neutral or charged state. Equally importantly, structural relaxations must be performed as defects will definitely cause local atomic distortions with different charge states. For a neutral defect under dilute approximation,

the formation energy can be accurately obtained using a sufficiently large supercell to eliminate the image interactions. For a charged defect,  $q$  electrons are removed from (added to) the defect and so are its periodic images. The long-range Coulomb interactions between the defect and its periodic images would induce a divergence of the total energy [20]. To remove such divergence, a so-called jellium model is routinely used with homogeneous background charge added to the whole supercell space to neutralize the supercell so that the total energy and the formation energy of a charged defect can be obtained. To eliminate the effect of the jellium charge on the defect formation energy, the following argument is often adopted: As the supercell size increases, the jellium charge density will go to zero and the charged defect formation energy will converge with supercell sizes when interactions of defect images are negligible. Once converged formation energies of neutral and charged defects are known, the IE of the defect can be calculated. During the past decades, this method has achieved great success to understand defect behaviors in 3D semiconductors [21–25].

Recently, low-dimensional (LD) semiconductors have attracted more and more research interest [26–31]. Consequently, the defect behaviors in low-dimensional systems, including two-dimensional (2D) monolayers and surfaces, and one-dimensional (1D) nanoribbons, nanowires, and nanotubes, are becoming more and more important to explore. During the past decades, people have tried to do so following the same treatment as that used for 3D semiconductors. Particularly, for a charged defect, a homogeneous background charge is added to the whole space of the slab model including the vacuum region [32,33]. While the formation energy of a

\*jhyang04@fudan.edu.cn

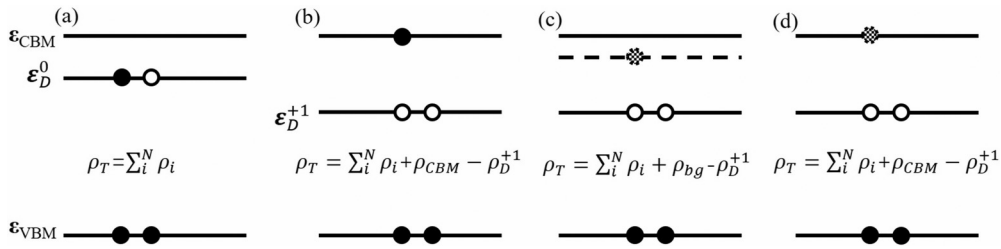


FIG. 1. Diagrams to show electron occupations for a donor in an infinitely large supercell at (a) the neutral state, (b) the charged ionized state, (c) the charged state in the conventional jellium model framework, and (d) the charged state in the present calculation. The charge density is given with  $\rho_i$ ,  $\rho_{CBM}$ ,  $\rho_{bg}$ , and  $\rho_D^{-1}$  standing for the charge density in the  $i$ th band, CBM, background, and charged defect level, respectively. The electrons and holes are represented by solid and hollow circles, respectively. Solid and dashed lines (circles) stand for real and virtual states (carriers), respectively.

neutral defect can easily converge by increasing the sizes of the supercell and vacuum regions, the formation energy of a charged defect is difficult or impossible to converge by increasing the size of the vacuum region, which is a well-known issue due to the Coulomb interactions between the charge in the vacuum and that in material regions. Besides, due to the unphysical jellium charge and the induced incorrect Coulomb potential, whether structures of charged defects obtained from the jellium model are reasonable or not remains unclarified. These two issues pose great challenges in studying defect properties of 2D semiconductors.

To solve the first issue, that is, the formation energy convergence problem, various methods have been tried, such as confining the background charge in a given region, introducing a neutralizing charge by using pseudoatoms, *posteriori* corrections to fix the potential at cell boundaries [34–38], etc. Based on the jellium model, Wang *et al.* derived an analytical form of IE as a function of supercell lattice parameters  $L_x$ ,  $L_y$ , and  $L_z$  for 2D semiconductors. They used an extrapolation method to obtain the converged values of IE's [33,39]. Alternatively, Wu, Zhang, and Pantelides (WZP) considered the physical process of defect ionization, in which electrons or holes will be removed from the neutral defect state and excited to the conduction bands or valance bands. Under the dilute limit of defects, the excited electrons or holes will occupy the conduction band minimum (CBM) or the valance band maximum (VBM) after thermodynamic equilibrium. Based on this process, they proposed to simulate the charged defect by constraining the electron occupation numbers at the defect state and the band edges [21]. By doing this, the defect is charged but the whole supercell is still neutral. Consequently, the total energy of such charged defect state has no divergence issue. Recently, Deng and Wei [41] proposed to simulate an ionized defect by transferring charge from the defect state to the real host band-edge state (denoted as TRSM) and they developed a corresponding method to calculate the total energies of supercells with charged defects. In general, the above methods can solve the formation energy convergence issue. However, the second issue, that is, structure relaxation of charged defects in LD semiconductors, is still an open question. In principle, both total energies and structure relaxations should be self-consistently obtained in one single calculation and in a physically meaningful way, which is still furnished in present studies as far as we know.

In this paper, we calculated the charged defect structures and ionization energies of LD semiconductors in a self-consistent way. We combine the jellium framework, that is, the number of occupied orbitals is the same as that in the jellium model, together with the idea of constraining charge transfer to deal with charged defects in LD semiconductors. By doing this, we show that the total electronic charge density is exactly the same as the real charge density for an ionized defect, thus ensuring the total energy is physically meaningful. More importantly, the jellium model framework ensures that the forces on atoms from the contribution of both charge densities and occupied wave functions are implicitly included, enabling a self-consistent performance of structure relaxation and total energy calculation in one single calculation. By studying defects in typical 2D materials such as BN, MoS<sub>2</sub>, and black phosphorus monolayers, we show that structure relaxation can contribute significantly to the final defect ionization energies. Our work thus provides a simple and efficient way to determine the charged defect structures and defect ionization energies in low-dimensional semiconductors.

## II. CALCULATION METHODOLOGY

In the following, we take a donor (denoted as  $\alpha$ ) as an example, to show how the the defect ionization is calculated in our scheme. The acceptor case is given in the Supplemental Material (Fig. S1) [40]. Before ionization, the donor state is neutral and below the CBM. Without loss of generality, let us suppose that it has one electron and one hole as shown in Fig. 1(a). All the states below the donor state are fully occupied by electrons at  $T = 0$ . Assume the total number of electrons in the system is  $N$ . Apparently, the whole system is a ground state and the total energy, denoted as  $E^N(\alpha, 0)$ , can be easily obtained from the ground-state calculations. After ionization, the defect donates one electron to the conduction band, leaving one hole behind. Under thermodynamical equilibrium condition and at the dilute limit of defects, the electron finally will be relaxed to the CBM state, as shown in Fig. 1(b). The ionized defect state is now an excited state of the  $N$ -electron system. Once we know the total energy of the excited state [denoted as  $\tilde{E}^N(\alpha, +1)$ ], the defect IE can then be calculated as  $\text{IE} = \tilde{E}^N(\alpha, +1) - E^N(\alpha, 0)$  according to its definition.

To obtain  $\tilde{E}^N(\alpha, +1)$ , one can directly follow the scheme in Fig. 1(b) and perform total energy calculations of charged defective supercells by constraining either charge transfer [41] or electron occupation [21] to reproduce real ionized defect states. However, before this, the structure relaxations of charged defects should be performed, which need to consider forces on atoms. Usually, forces are obtained from the Hellmann-Feynman theorem in modern first-principles calculations, which require not only charge densities but also wave functions of occupied states. For the case in Fig. 1(b),  $N$  wave functions of the occupied states, including the CBM state and the states below the defect state, should be used to calculate forces on the atoms. However, present defect calculations often use small supercells and therefore one cannot identify the exact CBM state. Consequently, how to choose  $N$  wave functions in Fig. 1(b) is difficult to address, leaving it as a problem to self-consistently and simultaneously perform structure relaxations of charged defects and calculate total energies in one single calculation.

Alternatively, one can calculate  $\tilde{E}^N(\alpha, +1)$  by making reasonable approximations. At the dilute limit of defects, i.e., in an infinitely large supercell, it is a good approximation that the band edges are not affected by the existence of a defect, which means that the contribution of this electron to the total energy of the supercell is just the CBM energy  $\varepsilon_{\text{CBM}}$ . Therefore,  $\tilde{E}^N(\alpha, +1)$  can be approximated as  $E^{N-1}(\alpha, +1) + \varepsilon_{\text{CBM}}$ , where  $E^{N-1}(\alpha, +1)$  is the total energy of the charged defective supercell. Then defect IE can be calculated as  $\text{IE} = E^{N-1}(\alpha, +1) - E^N(\alpha, 0) + \varepsilon_{\text{CBM}}$ . This formula has been widely used to calculate defect IEs in the past decades for 3D semiconductors.

Note that the charged defective supercell in Fig. 1(c) has  $(N - 1)$  electrons and  $Ne$  positive charge on the nuclei. To keep the whole system neutral and obtain converged  $E^{N-1}(\alpha, +1)$ , the jellium model is routinely adopted with a background charge uniformly distributed in the whole space of the charged defective supercell [42]. In a 3D system, the jellium charge can be seen as occupying a virtual state with an eigenenergy of the Fermi level of the system [Fig. 1(c)]. Note that, in modern defect calculations, the jellium charge density only plays a role during the solution of Poisson equations but is not considered during the calculation of exchange and correlation potentials. Therefore, in the conventional jellium model method shown in Fig. 1(c),  $(N - 1)$  electrons are used to calculate the exchange and correlation potentials but  $N$ -electron charge density is used to determine the Coulomb potential. However, when the conventional jellium model meets LD semiconductors, the jellium charge is distributed in the whole supercell space including material and vacuum regions, leading to the well-known divergence of formation energies for charged defects as well as defect IEs. Consequently, one has to look back at the physical reasonability of the defect IE calculation methods based on the conventional jellium model.

As we know, total energy is functionals of charge density in DFT. Therefore, if the charge density in a system is unphysical, the total energy and the related physical quantities might also be incorrect. In the conventional jellium model for a charged defect system, the charge has the following contributions:  $Ne$  positive charge from the nuclei,  $(N - 1)e$  negative charge from the electrons, and  $1e$  negative charge from the

jellium background. Compared to the real charge density of the ionized defect state [Fig. 1(b)], one can see that the  $1e$  negative jellium background charge is not physical. However, if we replace the unphysical jellium background charge in the conventional jellium model by the band-edge charge [i.e., VBM for acceptors or CBM for donors; see Fig. 1(d)], the electronic charge density will be restored back to the real charge density of the ionized defect state in Fig. 1(b), which has a clear physical meaning. In practice, this can be done by adding  $\Delta\rho = +\rho_{\text{CBM}}$  in each electronic iteration within the jellium model framework (here, we still use the same number of occupied orbitals as that in the jellium model). By doing this, we can see that  $N$ -electron charge density is used to determine the exchange and correlation potentials as well as the Coulomb potential, in agreement with the practical case shown in Fig. 1(b). Using the corrected charge density, the total energy of the charged defect system  $E_{\text{corr}}^{N-1}(\alpha, +1)$  can be calculated. Now at the dilute limit of defects,  $\tilde{E}^N(\alpha, +1)$  can be approximated as  $E_{\text{corr}}^{N-1}(\alpha, +1) + \varepsilon_{\text{CBM}}$  and the defect IE can be calculated as  $\text{IE} = E_{\text{corr}}^{N-1}(\alpha, +1) - E^N(\alpha, 0) + \varepsilon_{\text{CBM}}$ . Note that the sum of  $E_{\text{corr}}^{N-1}(\alpha, +1)$  and  $\varepsilon_{\text{CBM}}$  corresponds to  $\tilde{E}^N(\alpha, +1)$  in Fig. 1(b). The reason for adding  $\varepsilon_{\text{CBM}}$  is to correct the band energies as only  $(N-1)$  orbitals are taken into account to get the total energies in the jellium model framework.

Here we discuss how the forces should be dealt with. In the practical case shown in Fig. 1(b), as we mentioned above,  $(N - 1)$  wave functions below the defect states and the CBM wave function should be taken into account to calculate the forces on atoms. However, due to small supercells, the CBM wave function in defective systems cannot be identified in practical calculations. Fortunately, the CBM wave function is delocalized and thus it is reasonable to neglect the contributions of the CBM wave function to the forces. Finally, we can use  $N - 1$  wave functions and  $N$ -electron charge density, to obtain the forces on atoms, which is exactly performed in our scheme in Fig. 1(d). Consequently, the combination of the jellium model framework with the constrained charge transfer gives not only physically meaningful total energies but also reasonable forces, thus enabling a self-consistent determination of charged defect structures and total energies in one single calculation. Consequently, both the charged defect formation energy convergence issue and the charged defect structure relaxation issue can be solved using Fig. 1(d).

### III. FIRST-PRINCIPLES CALCULATION METHODS

Based on the above justification of Fig. 1(d) for defect IE calculations, we implement the scheme in QUANTUM ESPRESSO [43]. The charge density correction is done in each electronic iteration which guarantees its contribution to the potential energy and the total energy (the flow chart of our scheme is given in Fig. S2 in the Supplemental Material [40]). Structure relaxations are implicitly and self-consistently performed together with the total energy calculations. The norm-conserving pseudopotentials within the Perdew-Burke-Ernzerhof (PBE) framework [44–46] are used to treat the valence electrons. For the Brillouin zone integrals in the reciprocal space, a single  $\Gamma$  point is used for all calculations for

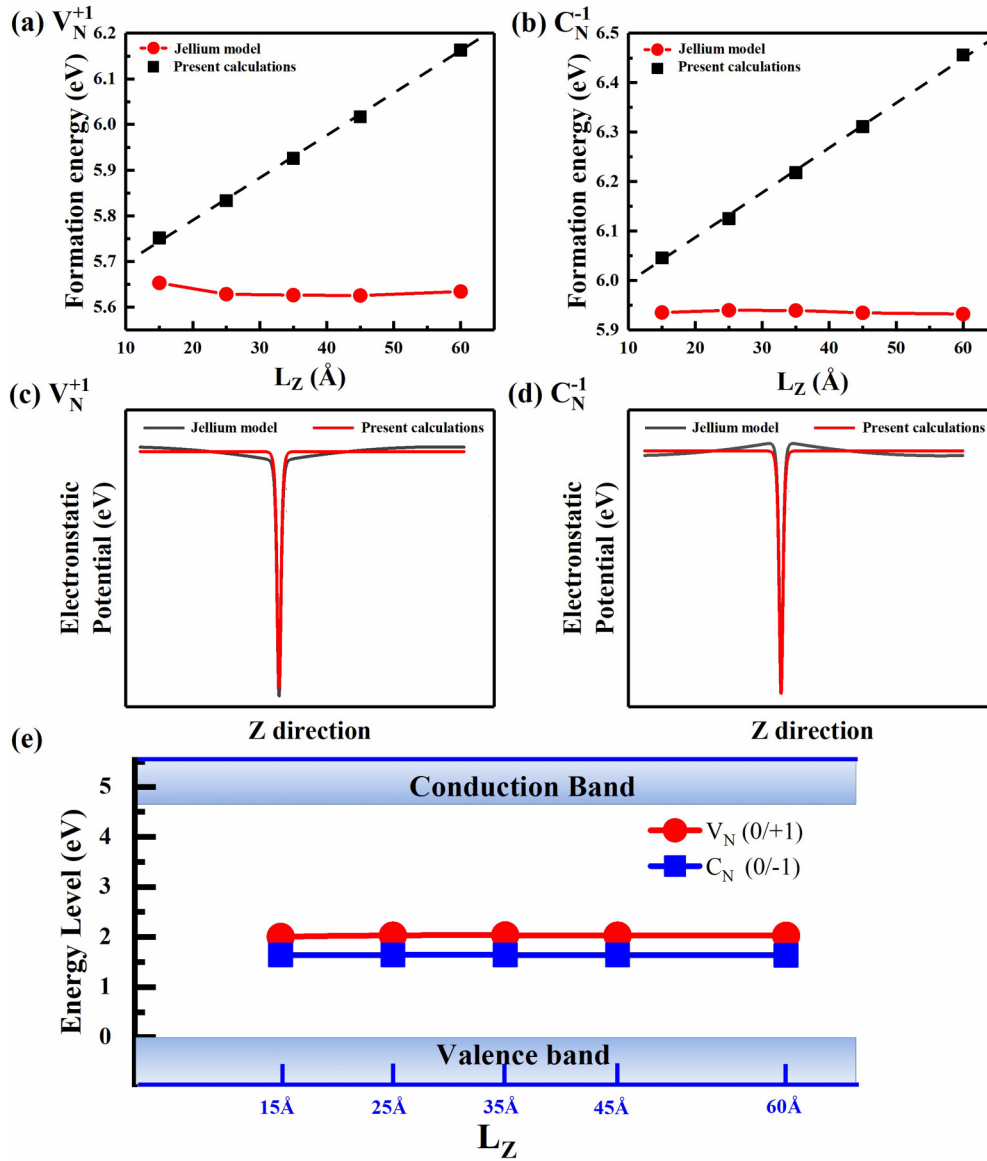


FIG. 2. Calculated defect properties of two-dimensional BN with the conventional jellium model method and our improved scheme. (a,b) Formation energies of  $V_N^+$  and  $C_N^-$  dependence on vacuum lengths. (c,d) Electrostatic potentials along the vacuum direction of  $V_N^+$  and  $C_N^-$  supercells with the lengths along vacuum directions fixed at 60 Å. (e) Defect IE's of  $V_N^+$  and  $C_N^-$  as functions of vacuum lengths. The lateral sizes of all supercells are fixed as  $12 \times 12$  of the primitive cells. Note that the (0/-) level of  $C_N^-$  is equal to its defect IE while the (0/+) level of  $V_N^+$  is equal to the band-gap value of BN minus the defect IE of  $V_N^+$ . The dashes lines are added as a guide for the eye.

simplicity. The kinetic energy cutoff energy of the plane wave basis is 90 Ry, and the total energy threshold for convergence is  $10^{-8}$  Ry. All atoms are relaxed until the Hellmann-Feynman forces on individual atoms are less than  $10^{-4}$  Ry/bohr. The VBM and CBM states are implicitly aligned to the levels in defective supercells using vacuum levels. To determine the defect formation energies, we calculate the total energy  $E(\alpha, q)$  for a supercell containing the relaxed defect  $\alpha$  in its charge state  $q$ . We also calculate the total energy  $E(\text{host})$  for the same supercell in the absence of the defect, as well as the total energies of elemental solids or gases at their stable phases. The defect formation energy  $\Delta H_f(\alpha, q)$  as a function of the electron Fermi energy  $E_F$  and the atomic chemical

potential  $\mu_i$  is given by [47]

$$\Delta H_f(\alpha, q) = \Delta E(\alpha, q) + \sum n_i \mu_i + qE_F, \quad (1)$$

where  $\Delta E(\alpha, q) = E(\alpha, q) - E(\text{host}) + n_i E(i) + qE_{\text{VBM}}$ ,  $E_F$  is referenced to the VBM of perfect systems, and  $\mu_i$  is the chemical potential of constituent  $i$  referenced to elemental solid or gas with energy  $E(i)$ . The  $n_i$  are the numbers of atoms taken out of the supercell to form the defects, and  $q$  is the number of electrons transferred from the supercell to the Fermi reservoirs in forming the defect cell. Here in the following, the defect formation energies are given by setting

$\mu_i$  and  $E_F$  as zeros unless otherwise specified. Note that, in our improved scheme,  $E(\alpha, q)$  is equal to  $\tilde{E}_{\text{corr}}^{N-1}(\alpha, +1)$ .

#### IV. RESULTS AND DISCUSSIONS

First, we demonstrate that using the implementation shown in Fig. 1(d), converged charge defect formation energies and defect IEs with respect to the sizes of vacuum regions are achieved for LD semiconductors. We take defects in the h-BN monolayer as examples and consider nitrogen vacancy ( $V_N$ ) and carbon substituting nitrogen ( $C_N$ ) as typical donor and acceptor defects, respectively. By fixing the lateral sizes of defective supercells as  $12 \times 12 \times 1$  of the primitive cells, Figs. 2(a) and 2(b) show the calculated formation energies of charged defects of  $V_N^+$  and  $C_N^-$  as functions of vacuum thickness. Clearly, in the conventional method based on the jellium model, the formation energies of  $V_N^+$  and  $C_N^-$  increase almost linearly with the length of vacuum regions, in agreement with previous reports [39]. Instead, using our improved scheme in Fig. 1(d), both the formation energies of  $V_N^+$  and  $C_N^-$  do not change with the vacuum thickness [Figs. 2(a) and 2(b)]. This can be understood as follows. In the conventional method, the uniformly distributed negative (positive) background charge for a charged donor (acceptor) increases (decreases) the electrostatic potentials in the vacuum regions [Figs. 2(c) and 2(d)]. For acceptor defects, if the electrostatic potentials drop too much to make the vacuum level lower than the states in the material regions, electrons will transfer from material regions to the vacuum [39], causing the deviation of defect formation energies from linear increase with vacuum thickness (see also Fig. S3 [40]). In the present scheme, there is no background charge in the vacuum regions and thus the electron electrostatic potentials are rather flat [see Fig. 2(b)], leading to the unchanged formation energies for charged defects with respect to vacuum thickness. Consequently, the defect IEs are also converged with respect to vacuum sizes, as shown in Fig. 2(e).

Next, we consider the effects of finite lateral supercell sizes on defect IEs. Because of PBCs, there are long-range Coulomb interactions between the charged defect and its images. Therefore, convergence of defect IEs also needs to be achieved with respect to the lateral supercell sizes. By fixing the vacuum thickness as  $15 \text{ \AA}$ , we gradually increase the lateral sizes of defect supercells from  $3 \times 3$  to  $15 \times 15$  of the primitive cells. As can be seen in Fig. 3, the calculated defect IEs using Fig. 1(d) have been converged within  $0.1 \text{ eV}$

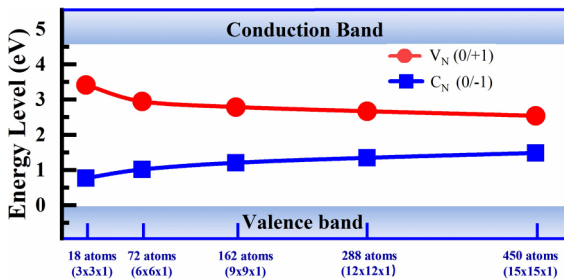


FIG. 3. Defect IE's of  $V_N^+$  and  $C_N^-$  as functions of lateral supercell sizes with the supercell length along the vacuum direction fixed at  $15 \text{ \AA}$ .

TABLE I. Calculated defect IEs in some typical 2D semiconductors using our improved scheme in comparison with available references using conventional methods based on the jellium model.

| Systems                   | Defect    | Charge state | IE (eV) | References (eV)      |
|---------------------------|-----------|--------------|---------|----------------------|
| 2D BN                     | $V_B$     | -1           | 0.965   | 1.44 [39]            |
|                           | $V_N$     | +1           | 2.016   | 2.50 [39]            |
|                           | $C_B$     | +1           | 1.598   | 2.03 [39], 2.24 [48] |
|                           | $C_N$     | -1           | 1.394   | 1.86 [39], 2.03 [48] |
| Quasi-2D BP               | $O_P$     | +1           | 0.782   | >0.91 [33]           |
|                           | $S_P$     | +1           | 0.487   | 0.74 [33]            |
|                           | $Se_P$    | +1           | 0.437   | 0.69 [33]            |
|                           | $Te_P$    | +1           | 0.344   | 0.67 [33]            |
| Quasi-2D MoS <sub>2</sub> | $V_S$     | -1           | 1.345   | 1.40 [49]            |
|                           | $V_{Mo}$  | -1           | 0.712   | 0.85 [49]            |
|                           | $Re_{Mo}$ | +1           | 0.112   | 0.22 [49]            |
|                           | $F_S$     | +1           | 0.326   | 0.65 [49]            |

using a  $12 \times 12$  supercell, which is a typical supercell size in modern defect calculations with affordable computational costs. Combining the results in both Figs. 2 and 3, we can conclude that the present scheme of dealing with charged defects in LD semiconductors has eliminated the divergence problem in the conventional method based on the jellium model.

Using the newly developed scheme, we have studied defect properties of several typical 2D semiconductors including BN, black phosphorus, and MoS<sub>2</sub> monolayers. The calculated defect IE's are listed in Table I, in comparison with available results of other methods based on the jellium model. We notice that our calculated defect IEs are systematically smaller than those using the methods based on the jellium model. This can be simply understood from the Coulomb interactions between the background charge and the charge in the material regions. In the present scheme, the background charge density is physically meaningful band-edge charge density, which is distributed only within the materials. On the other hand, the background charge density in the jellium model is distributed in the whole space. As a result, the Coulomb interaction between the background and the material charge is stronger in our scheme. As the background charge has an opposite sign to the net charge in the material regions, the total energies of charged defective supercells in our scheme are smaller, giving smaller defect IEs and indicating previous works might have systematically overestimated defect IEs.

In addition to the defect IEs, we also analyze the structure relaxations before and after defect ionizations obtained using our improved scheme. The changes of bond lengths between the defective atoms and their neighboring atoms for defects in BN and BP monolayers are given in Table II as well as the energy contribution to defect IEs due to structure relaxation (denoted as  $IE_{\text{relax}}$ ). For defects in BN, the lengths of three bonds ( $d_1$ ,  $d_2$ , and  $d_3$  in Fig. 4) are the same because of symmetry. As seen in Table II, the changes of bond lengths due to defect ionizations are around  $0.035 \text{ \AA}$ , which contributes to defect IEs by as much as  $0.3 \text{ eV}$  (see Table II), demonstrating that structure relaxations are very important to determine final defect IE's. For defects in the BP monolayer, the situation is somewhat different. Because atoms in the BP monolayer are

TABLE II. Calculated changes of bond lengths between defective atoms and neighboring atoms due to defect ionization using our improved scheme in comparisons with those obtained using the conventional jellium model. The energy changes due to structure relaxations of charged defects are listed as  $IE_{\text{relax}}$ .

| Systems     | Defect | Charge state | $\Delta$ Length, ours ( $\text{\AA}$ ) | $\Delta$ Length, jellium ( $\text{\AA}$ ) | $IE_{\text{relax}}$ , ours (eV) | $IE_{\text{relax}}$ , jellium (eV) |
|-------------|--------|--------------|--|---|---------------------------------|------------------------------------|
| 2D-BN       | $C_B$  | +1           | -0.027                                 | -0.027                                    | -0.300                          | -0.300                             |
|             | $C_N$  | -1           | -0.038                                 | -0.039                                    | -0.278                          | -0.282                             |
| Quasi-2D BP | $O_P$  | +1           | 0.001, 0.117                           | 0.001, 0.048                              | -0.017                          | -0.025                             |
|             | $S_P$  | +1           | 0.037, -0.581                          | 0.040, -0.590                             | -0.200                          | -0.208                             |
|             | $Se_P$ | +1           | 0.034, -0.478                          | 0.036, -0.487                             | -0.198                          | -0.204                             |
|             | $Te_P$ | +1           | 0.016, -0.367                          | 0.016, -0.372                             | -0.179                          | -0.185                             |

no longer in the same plane, defect atoms have a larger degree of freedom and the bond lengths around defects are divided into two kinds, i.e., the bonding of atoms in the same plane (such as  $d_2$  and  $d_3$  in Fig. 4) and the bonding between atoms in different planes (such as  $d_1$  in Fig. 4). While changes of  $d_2$  and  $d_3$  are relatively small, changes of  $d_1$  are much larger. As seen in Table II, the changes of  $d_1$  are as large as 0.500  $\text{\AA}$ . Such large structure relaxation contributes to defect IEs by as much as 0.2 eV. Note that  $IE_{\text{relax}}$  in the BP monolayer has reached 50% of the final defect IEs. Consequently, structure relaxation due to defect ionization plays important roles in determining defect IEs and thus should be dealt with carefully.

Because structure relaxation of charged defects is often considered using the jellium model in previous methods, here we compare our results of structure relaxations with those obtained using the jellium model. In general, the jellium model gives similar results of bond length changes and relaxation

energies compared to our calculations (see Table II). This can be understood from the following two facts. First, both our scheme and the jellium model use the wave functions of the same occupied states to calculate the forces. Second, the charge density used to calculate the forces in our calculations is very similar to that used in the jellium model because the distributions of band-edge charge and the homogeneous jellium charge are both delocalized in BN and BP monolayers. However, if the band-edge charge distribution is quite different from the jellium charge, the difference of structure relaxation can be larger. In fact, such situations do exist in LD semiconductors. For example, in 1D nanowires, the VBM can be distributed in the inner part of the nanowire while the CBM is in the outer part or vice versa. In this case, the structure relaxation of charged defects given by the jellium model may be not accurate enough and should be carefully considered.

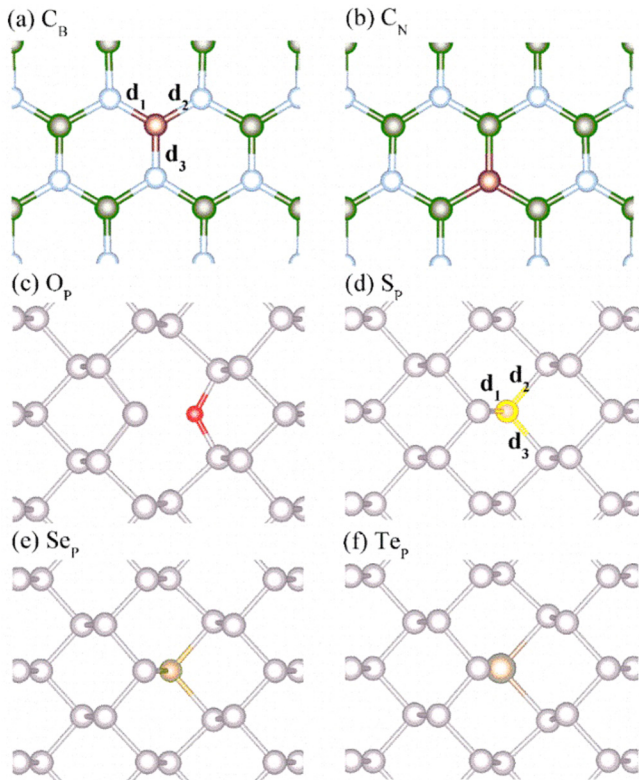


FIG. 4. Fully relaxed structures of charged defects. (a, b) Top view of relaxed defect structures in BN monolayer. (c-f) Top view of relaxed defect structures in the BP monolayer.

## V. SUMMARY

In summary, by combining the jellium framework together with the idea of calculating total energies of ionized defect supercells by constraining charge transfer, we have realized the performance of the structure relaxation and total energy of ionized defect supercells self-consistently in one single calculation. We have justified our scheme and demonstrated it can eliminate the divergence issue in the conventional jellium methods to determine defect IEs. By studying defects in typical 2D materials, we have shown that structure relaxations can contribute significantly to the final defect IEs and thus should be considered in accordance with the total energy calculations. Our work thus provides a simple and efficient way to determine the structures of charged defects and defect ionization energies in low-dimensional semiconductors.

## ACKNOWLEDGMENTS

We appreciate useful discussions with Professor Su-Huai Wei from Beijing Computational Science Research Center. This work was supported in part by National Natural Science Foundation of China (Grant No. 11974078), Fudan Start-up funding (Grant No. JIH1512034), and Shanghai Sailing Program (Grant No. 19YF1403100). Calculations are performed at the High-Performance Computing Center of Fudan University.

- [1] S. Zhang, *J. Phys.: Condens. Matter* **14**, R881 (2002).
- [2] C. Freysoldt, B. Grabowski, T. Hickel, J. Neugebauer, G. Kresse, A. Janotti, and C. G. Van de Walle, *Rev. Mod. Phys.* **86**, 253 (2014).
- [3] Y. Peng, C. Xia, H. Zhang, T. Wang, S. Wei, and Y. Jia, *Phys. Chem. Chem. Phys.* **16**, 18799 (2014).
- [4] T. Gfroerer, Y. Zhang, and M. Wanlass, *Appl. Phys. Lett.* **102**, 012114 (2013).
- [5] J. Li, Z.-K. Yuan, S. Chen, X.-G. Gong, and S.-H. Wei, *Chem. Mater.* **31**, 826 (2019).
- [6] J. Weber, W. Koehl, J. Varley, A. Janotti, B. Buckley, C. Van de Walle, and D. D. Awschalom, *Proc. Natl. Acad. Sci. USA* **107**, 8513 (2010).
- [7] F. Oba, A. Togo, I. Tanaka, J. Paier, and G. Kresse, *Phys. Rev. B* **77**, 245202 (2008).
- [8] C. G. Van de Walle and J. Neugebauer, *J. Appl. Phys.* **95**, 3851 (2004).
- [9] A. Alkauskas, M. D. McCluskey, and C. G. Van de Walle, *J. Appl. Phys.* **119**, 181101 (2016).
- [10] E. G. Seebauer and M. C. Kratzer, *Mater. Sci. Eng., R* **55**, 57 (2006).
- [11] C. W. M. Castleton, A. Höglund, and S. Mirbt, *Phys. Rev. B* **73**, 035215 (2006).
- [12] J. Shim, E.-K. Lee, Y. J. Lee, and R. M. Nieminen, *Phys. Rev. B* **71**, 035206 (2005).
- [13] A. Wright and N. Modine, *Phys. Rev. B* **74**, 235209 (2006).
- [14] M. Leslie and N. Gillan, *J. Phys. C: Solid State Phys.* **18**, 973 (1985).
- [15] A. Walsh, S. Chen, S.-H. Wei, and X.-G. Gong, *Adv. Energy Mater.* **2**, 400 (2012).
- [16] W. R. L. Lambrecht, *Phys. Status Solidi B* **248**, 1547 (2011).
- [17] J.-Y. Noh, H. Kim, and Y.-S. Kim, *Phys. Rev. B* **89**, 205417 (2014).
- [18] J.-Y. Noh, H. Kim, M. Park, and Y.-S. Kim, *Phys. Rev. B* **92**, 115431 (2015).
- [19] L. G. Wang and A. Zunger, *Phys. Rev. B* **66**, 161202(R) (2002).
- [20] H. P. Komsa and A. Pasquarello, *Phys. Rev. Lett.* **110**, 095505 (2013).
- [21] Y.-N. Wu, X. G. Zhang, and S. T. Pantelides, *Phys. Rev. Lett.* **119**, 105501 (2017).
- [22] H. X. Deng and S. H. Wei, *Phys. Rev. Lett.* **120**, 039601 (2018).
- [23] W. Chen and A. Pasquarello, *Phys. Rev. Lett.* **120**, 039603 (2018).
- [24] Y. N. Wu, X. G. Zhang, and S. T. Pantelides, *Phys. Rev. Lett.* **120**, 039604 (2018).
- [25] Y. N. Wu, X. G. Zhang, and S. T. Pantelides, *Phys. Rev. Lett.* **120**, 039602 (2018).
- [26] M. Xu, T. Liang, M. Shi, and H. Chen, *Chem. Rev.* **113**, 3766 (2013).
- [27] G. Slotman and A. Fasolino, *J. Phys.: Condens. Matter* **25**, 045009 (2012).
- [28] B. Radisavljevic, A. Radenovic, J. Brivio, V. Giacometti, and A. Kis, *Nat. Nanotechnol.* **6**, 147 (2011).
- [29] S. B. Desai, S. R. Madhupathy, A. B. Sachid, J. P. Llinas, Q. Wang, G. H. Ahn, G. Pitner, M. J. Kim, J. Bokor, C. Hu *et al.*, *Science* **354**, 99 (2016).
- [30] J. S. Qiao, X. H. Kong, Z. X. Hu, F. Yang, and W. Ji, *Nat. Commun.* **5**, 4475 (2014).
- [31] H. Liu, A. T. Neal, Z. Zhu, Z. Luo, X. Xu, D. Tománek, and P. D. Ye, *ACS Nano* **8**, 4033 (2014).
- [32] D. Wang, X.-B. Li, D. Han, W. Q. Tian, and H.-B. Sun, *Nano Today* **16**, 30 (2017).
- [33] D. Wang, D. Han, X.-B. Li, N.-K. Chen, D. West, V. Meunier, S. Zhang, and H.-B. Sun, *Phys. Rev. B* **96**, 155424 (2017).
- [34] I. Dabo, B. Kozinsky, N. E. Singh-Miller, and N. Marzari, *Phys. Rev. B* **77**, 115139 (2008).
- [35] O. Sinai and L. Kronik, *Phys. Rev. B* **87**, 235305 (2013).
- [36] N. A. Richter, S. Siculo, S. V. Levchenko, J. Sauer, and M. Scheffler, *Phys. Rev. Lett.* **111**, 045502 (2013).
- [37] T. Cao and A. Bongiorno, *Sci. Rep.* **7**, 2834 (2017).
- [38] P. Pulay, *Mol Phys.* **100**, 57 (2002).
- [39] D. Wang, D. Han, X. B. Li, S. Y. Xie, N. K. Chen, W. Q. Tian, D. West, H. B. Sun, and S. B. Zhang, *Phys. Rev. Lett.* **114**, 196801 (2015).
- [40] See Supplemental Material at <http://link.aps.org/supplemental/10.1103/PhysRevB.102.035202> for the acceptor case and details of the self-consistent loop process in our scheme.
- [41] J. Xiao, K. K. Yang, D. Guo, T. Shen, H. X. Deng, S. S. Li, J. W. Luo, and S. H. Wei, *Phys. Rev. B* **101**, 165306 (2020).
- [42] C. G. Van de Walle, P. J. H. Denteneer, Y. Bar-Yam, and S. T. Pantelides, *Phys. Rev. B* **39**, 10791 (1989).
- [43] P. Giannozzi, S. Baroni, N. Bonini, M. Calandra, R. Car, C. Cavazzoni, D. Ceresoli, G. L. Chiarotti, M. Cococcioni, I. Dabo *et al.*, *J. Phys.: Condens. Matter* **21**, 395502 (2009).
- [44] P. E. Blöchl, *Phys. Rev. B* **50**, 17953 (1994).
- [45] G. Kresse and D. Joubert, *Phys. Rev. B* **59**, 1758 (1999).
- [46] J. P. Perdew, K. Burke, and M. Ernzerhof, *Phys. Rev. Lett.* **77**, 3865 (1996).
- [47] S.-H. Wei, *Comput. Mater. Sci.* **30**, 337 (2004).
- [48] H.-P. Komsa, N. Berseneva, A. V. Krasheninnikov, and R. M. Nieminen, *Phys. Rev. X* **4**, 031044 (2014).
- [49] H.-P. Komsa and A. V. Krasheninnikov, *Phys. Rev. B* **91**, 125304 (2015).